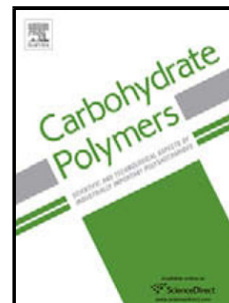


Journal Pre-proof

Hyaluronic acid-based levofloxacin nanomicelles for nitric oxide-triggered drug delivery to treat bacterial infections

Chunbo Lu, Yao Xiao, Yinyin Liu, Feifei Sun, Yuanhao Qiu, Haibo Mu, Jinyou Duan



PII: S0144-8617(19)31147-6

DOI: <https://doi.org/10.1016/j.carbpol.2019.115479>

Reference: CARP 115479

To appear in: *Carbohydrate Polymers*

Received Date: 13 June 2019

Revised Date: 14 October 2019

Accepted Date: 14 October 2019

Please cite this article as: Lu C, Xiao Y, Liu Y, Sun F, Qiu Y, Mu H, Duan J, Hyaluronic acid-based levofloxacin nanomicelles for nitric oxide-triggered drug delivery to treat bacterial infections, *Carbohydrate Polymers* (2019), doi: <https://doi.org/10.1016/j.carbpol.2019.115479>

This is a PDF file of an article that has undergone enhancements after acceptance, such as the addition of a cover page and metadata, and formatting for readability, but it is not yet the definitive version of record. This version will undergo additional copyediting, typesetting and review before it is published in its final form, but we are providing this version to give early visibility of the article. Please note that, during the production process, errors may be discovered which could affect the content, and all legal disclaimers that apply to the journal pertain.

© 2019 Published by Elsevier.

Hyaluronic acid-based levofloxacin nanomicelles for nitric oxide-triggered drug delivery to treat bacterial infections

Chunbo Lu,† Yao Xiao,† Yinyin Liu, Feifei Sun , Yuanhao Qiu, Haibo Mu*, Jinyou Duan *

Author Affiliations:

College of Chemistry & Pharmacy, Shaanxi Key Laboratory of Natural Products & Chemical Biology, Northwest A&F University, Yangling 712100, Shaanxi, China

† These authors contributed equally to this work.

*Corresponding author:

E-mail addresses: mhb1025@nwsuaf.edu.cn (H. Mu), jduan@nwsuaf.edu.cn (J. Duan).

Tel.: +86 29 87092226; Fax: +86 29 87092226

Highlights:

- Levofloxacin conjugated hyaluronic acid was synthesized by *o*-phenylenediamine group linkage.
- HA-NO-LF nanomicelles could enter macrophages via a CD44 mediated endocytosis.
- HA-NO-LF nanomicelles showed better bactericidal effects against *S. aureus* than LF *in vivo*.

Abstract

Antibiotics are powerful weapons to fight against bacterial infections, while most of them lack of selective targeting towards pathological site which could restrict their antibacterial efficacy. To overcome this challenge, an antimicrobial levofloxacin (LF)

was conjugated onto hyaluronic acid (HA) moieties via an *o*-phenylenediamine linker to prepare a NO-sensitive nanosystem (HA-NO-LF) in this study. The HA-NO-LF nanomicelles could enter host cells via a CD44 mediated endocytosis and release drug gradually upon exposure to endogenous NO. Furthermore, the more promising therapeutic effect of the nanomicelles in ameliorating inflammatory levels was observed in a mouse pneumonia model than that of LF. These results suggest that the HA-NO-LF nanomicelles may exert potent curative effect in infectious diseases.

Keywords: Hyaluronic acid; NO-sensitivity; Nanomicelles; Drug release;

1. Introduction

Infectious diseases caused by pathogenic microorganisms have long been a prevalent threat to human health (Gao, Thamphiwatana, Angsantikul, & Zhang, 2014). The discovery and application of antibiotics has created a new era of human resistance to infectious diseases. It is well-documented that antibiotics are powerful weapons to fight against bacterial infections due to their high sterilization efficiency, broad spectrum applications, and low cost. However, most of them are effective only at a very high dose owing to the lack of selective targeting towards pathological sites, which could not only induce multiple drug resistance in microbes but also cause side effects to other tissues and organs (Chen et al., 2018). Accordingly, to combat infectious diseases efficiently, there is an urgent need for antimicrobial agents to achieve targeted delivery and controlled drug release towards the lesion sites, thus improving therapeutic effects and avoiding tissue injury or organ dysfunction.

Hyaluronic acid (HA), known as a natural linear polysaccharide with outstanding biodegradability, low toxicity and high water-affinity, has been extensively applied in biomedical field. Besides, the presence of multiple acid and hydroxyl groups in the HA molecules makes it an ideal candidate for chemical modification. Recently, scientists have paid more attention to HA as a drug carrier since it can bind to CD44 on the surface of certain cells (Huang & Huang, 2018). Specifically, CD44 is a type I transmembrane glycoprotein that is highly expressed on endothelial and mesenchymal

cells, especially in inflamed tissues (McDonald & Kubes, 2015). During the process of pathogenic attack, inflammatory reactions occur as an adaptive defense response in the organism. In this way, HA is expected to achieve targeted drug delivery as a carrier of antibiotics, thus increasing the effective dose of drug at inflammatory site and minimizing the side-effects due to overusing of antibiotics.

Recently, the functional polymer-based nanosystem has been elegantly designed to enable responsiveness to biological signaling molecules including reactive oxygen species (ROS) (Xu et al., 2017), hydrogen sulfide (H₂S) (Ma, Zheng, Zhang, & Xing, 2018) and nitric oxide (NO) (Yeo et al., 2019). It has been scientifically proven that macrophages secrete a large amount of NO by activating an inducible nitric oxide synthases (NOS) enzyme in inflammation process (Hoey, Grabowski, Ralston, Forrester, & Liversidge, 1997). Appropriate levels of NO influences critically important physiological activities including apoptosis, antiseptis and inflammatory regulation, while excessive NO is thought to be involved in the pathogenesis of severe diseases such as rheumatoid arthritis (RA), hypertension and cancer (Coussens & Werb, 2002). In that sense, harnessing endogenous NO to cleave synthetic HA-based nanosystem will open up great potential not only for triggered “on-demand” drug release but also removal of redundant NO radicals to prevent tissue damage.

Herein, to realize targeted delivery and controlled release of antibiotics, the NO-sensitive HA-based nanomicelles were developed via modification with NO-reactive moieties. It has been reported that the *o*-phenylenediamine group has been frequently utilized as a NO-sensitive unit due to its highly reactive nature toward NO (J. Hu et al., 2014; Jinming Hu, Whittaker, Yu, Quinn, & Davis, 2015; Park, Pramanick, Kim, Lee, & Kim, 2017). Levofloxacin (LF), a third-generation fluoroquinolone antibiotic effective against both Gram-positive and Gram-negative bacteria was selected as a model antibiotic in this study. The hypothesized NO-triggered nanomicelles (HA-NO-LF) were prepared by linking a hydrophilic HA chain and a lipophilic LF chain via a functionalized intermediate bearing *o*-phenylenediamine groups, followed

by self-assembly in aqueous condition. When encountered with NO, the *o*-phenylenediamine moieties could be transformed into benzotriazole moieties in a highly efficient manner, facilitating chain scission and propelling release of LF gradually. The properties of the nanomicelles including morphology, biocompatibility, NO-sensitive behavior as well as antibacterial effects were investigated *in vitro*. To further evaluate the therapeutic efficacy *in vivo*, pneumonia mice infected by *Staphylococcus aureus* were selected as the infectious model.

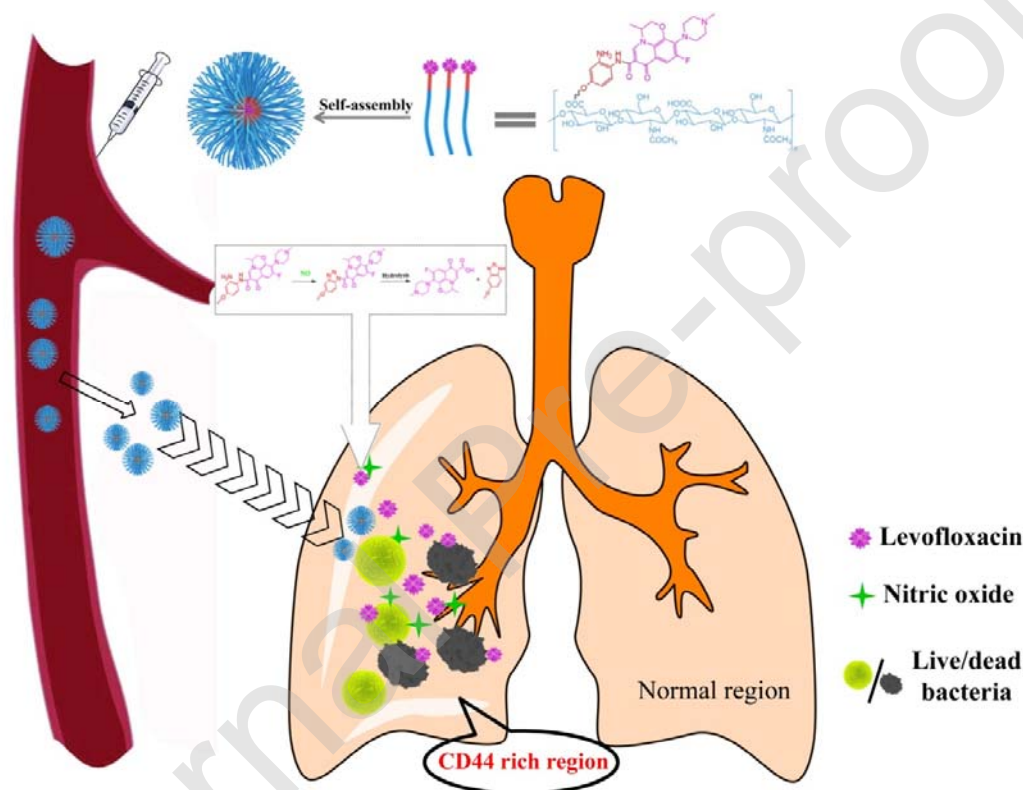


Fig.1 Schematic illustration of the proposed NO-triggered hyaluronic acid-levofloxacin nanomicelles targeting infection site.

2. Experimental and methods

2.1. Materials

Sodium hyaluronate (10 kDa) was bought from QuFu GuangLong Biochem Co., Ltd. Tetrabutylammonium hydroxide (TBAH), 3-nitro-4-amino-phenol (NA) 1,3-dibromopropane (DP), levofloxacin (LF) were purchased from Aladdin Chemical Reagent Company, China. N ω -Nitro-L-arginine methyl ester hydrochloride

(L-NAME), 3-(4,5-dimethylthiazol-2-yl)-2,5-diphenyl tetrazolium bromide (MTT), glutaraldehyde solution were obtained from Sigma Co. (St. Louis, MO, USA). All of other chemical reagents and solvents were of analytical grade and were used without further purification.

Staphylococcus aureus (ATCC 29213) and RAW 264.7 cells were generous gifts received from Prof. Xia (College of Food Science and Engineering, Northwest A&F University). Kunming mice were obtained from Experimental Animal Center of Basic Medical College, Xi'an Jiaotong University, China. This study was performed with the approval of the Experimental Animal Manage Committee (EAMC) of Northwest A&F University. Animals were treated as the guidelines of EAMC.

2.2. Preparation of HA-NO-LF conjugates

2.2.1. Synthesis of NA-DP

NA-DP was synthesized according to a reported procedure with slight modifications (Jinming Hu et al., 2015). NA (385 mg, 2.5 mmol) was previously dissolved in 50 mL acetone in a conical flask equipped with a magnetic bar, then K_2CO_3 (345 mg, 2.5 mmol) and DP (606 mg, 3 mmol) were added respectively. The reaction continuously proceeded for 36 h at 80 °C with gentle agitation. Further, the crude product was purified using silica gel column chromatography with ethyl acetate/petroleum ether as eluent to yield a red solid (526 mg, 76.5%) named NA-DP. **1H NMR (500 MHz, d-DMSO):** δ = 7.38 (d, J = 8.0 Hz, 1H), 7.24 - 7.16 (m, 2H), 7.00 (d, J = 8.5 Hz, 1H), 4.02 (t, J = 6.0 Hz, 2H), 3.65 (t, J = 6.0 Hz, 2H), 2.24 - 2.19 (m, 2H).

2.2.2. Synthesis of LF-NA-DP

LF-NA-DP conjugates were prepared by chemical grafting chlorinated levofloxacin (LF-Cl) to NA-DP through amide formation as previously described with minor modifications (Jinming Hu et al., 2015; Tomišić, Kujundžić, Krajačić, Višnjevac, & Kojić-Prodić, 2002). In detail, to obtain LF-Cl, LF (722 mg, 2 mmol) was dissolved in 50 mL anhydrous CH_2Cl_2 , and an appropriate amount of $SOCl_2$ was

added dropwise in an ice bath, followed by stirring overnight under N₂ atmosphere. Eventually, the mixture was concentrated under reduced pressure using a rotary evaporator at 45 °C to remove unreacted CH₂Cl₂ in dispersions. The freshly prepared LF-Cl (380 mg, 1 mmol) and moderate content of DIEA were then added to CH₂Cl₂ solution containing NA-DP (330 mg, 1.2 mmol) and stirred overnight at room temperature to ensure complete reaction. And the resulting solution was passed through a silica gel column chromatography (eluted with CH₂Cl₂/CH₃OH) to give the pure LF-NA-DP (422 mg, yield: 68.3%). **¹H NMR (500 MHz, d-DMSO):** δ = 12.94 (s, 1H), 8.94 (s, 1H), 8.38 (d, *J* = 8.5 Hz, 1H), 7.65 (s, 1H), 7.44 (d, *J* = 8.5 Hz, 1H), 4.93 (s, 1H), 4.60 (d, *J* = 10.5 Hz, 1H), 4.22 (d, *J* = 10.5 Hz, 1H), 4.22 (s, 2H), 3.72 (s, 2H), 3.00-2.86 (m, 4H), 2.61 (s, 2H), 2.53 (s, 5H), 2.32-2.94 (m, 2H), 1.48 (d, *J* = 4.5 Hz, 3H) .

2.2.3. Synthesis of HA-TBAH

Following a reported method (Sun et al., 2019), sodium hyaluronate was dissolved in distilled water to meet designated concentrations (50 mg/mL) and treated with a cationic-exchange resin (H⁺ form). Then the above solution was adjusted to the desired pH 7 by TBAH, resulting in the ideal product HA-TBAH.

2.2.4. Synthesis of HA-NO-LF

The lyophilized HA-TBAH (200 mg) was dissolved in dry DMSO, followed by dropping of LF-NA-DP (278 mg, 0.45 mmol) in the mixture. The reaction was incubated for 48 h at room temperature under stirring, and the resulting solution was dialyzed (MWCO 3500 Da) exhaustively against distilled water and then 0.1 M NaCl to remove impurities. Finally, the polymer solutions were lyophilized to obtain a sponge-like solid and stored at 4 °C for further use. Moreover, the solid above was redissolved in 20 mL of distilled water, after sequential addition of methanol and acetic acid at an appropriate amount, zinc powder was progressively added under stirring vigorously. The mixture was stirred for a further 1 h after the solution turned colorless to ensure the successful synthesis of NO-triggered conjugates. Then the final

product was purified and collected following the same procedure as conducted before, which was designated as HA-NO-LF.

LF content in the nanomicelles was determined by UV-Vis measurements as detailed described in supplementary information.

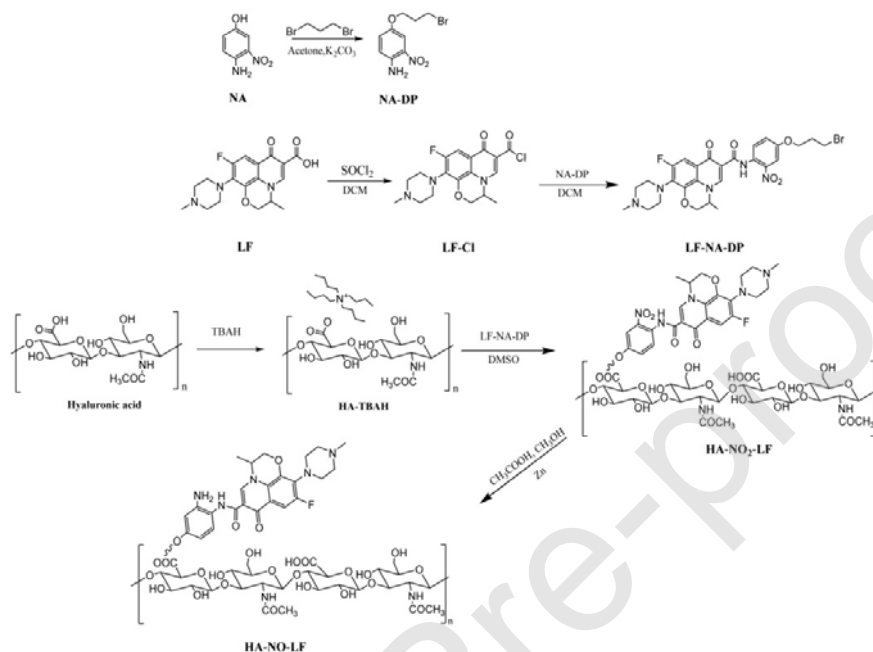


Fig.2 Synthetic routes of HA-NO-LF conjugates.

2.3. Characterization of HA-NA-LF conjugates

The UV-Vis spectra of HA, LF and HA-NO-LF were acquired on a Thermo Evolution 300 spectrophotometer in the range of 250-450 nm, respectively.

¹H NMR and ¹³C NMR spectra of the prepared conjugates were measured on a Bruker AM 500 spectrometer with reference to the chemical shift of the solvent peak. Chloroform (CDCl₃), deuterium oxide (D₂O) and d-DMSO were used as the solvents, depending on the particular substance being analyzed. FT-IR spectrophotometer (BRUKER TEMSOR 27, Germany) was employed to determine the intramolecular interactions between different components in the prepared conjugates with a resolution of 4 cm⁻¹, scanning from 500 to 4000 cm⁻¹ wavenumber.

2.4. Preparation and characterization of HA-NO-LF nanomicelles

2.4.1. Preparation of HA-NO-LF nanomicelles

In an attempt to prepare HA-NO-LF nanomicelles, 20 mg of HA-NO-LF conjugates were re-dissolved in 15 mL of DMSO. Then the solution was sonicated for 5 min using an ultrasonic cleaner (SB 5200-D; Ningbo Scientz Biotechnology Co., Ltd, Nanjing, China) at 200 W to ensure the uniform dispersion of nanoparticles. Finally, the solution was dialyzed against deionized water by using a dialysis bag with 3500 Da molecular cutoff for 3 days to obtain HA-NO-LF nanomicelles.

2.4.2. Characterization of HA-NO-LF nanomicelles

The particle size and zeta potential of freshly prepared nanomicelles were measured by dynamic light scattering (DLS) using a Malvern Nano ZetaSizer ZS model (Malvern Zetasizer NANOZS90, Malvern Instruments, Ltd., UK). Prior to each measurement, the samples were diluted with pure water to meet optimal instrument sensitivity. In addition, the stability of prepared nanomicelles stored in refrigerator at 4 °C were checked for particle size and zeta potential at predetermined intervals (0, 0.5, 1, 2, 3, 4, 5 and 6 days). The morphology of the HA-NO-LF micelles was characterized by Hitachi S-4800 field emission scanning electron microscopy (SEM) with an accelerating voltage of 10 kV (Hitachi, Japan).

2.5. *In vitro* drug release behavior

A dialysis membrane method was employed for quantitatively analyzing the kinetic release profile of LF from nanomicelles. Briefly, PBS buffer saturated with NO was prepared as release medium for LF (Liu, Hu, Whittaker, Davis, & Boyd, 2017). Then a dialysis bag (MWCO 3500 Da) containing 5 mL HA-NO-LF nanomicelles was immersed in 30 mL PBS (10mM, pH 7.4) at 37 °C. Noticeable, the PBS buffer containing saturated NO was continually applied after 6 h. Furthermore, 2 mL of release medium was collected at scheduled time intervals for measurement and fresh release medium was replenished to maintain the constant volume. And the same procedure was performed without NO as control. The absorbance of these samples at 293 nm was recorded using a UV-vis spectrophotometer to determine the percentage of released drug.

2.6. *In vitro* NO-sensitive antibacterial assay

The NO-sensitive antibacterial assay of HA-NO-LF nanomicelles against *S. aureus* was performed by following the method of Mu et al. (Mu, Liu, Niu, Sun, & Duan, 2016) with slight modifications. In detail, *S. aureus* strain was first grown in broth for 12 h, and then centrifuged at 5000 rpm and washed three times with PBS buffer to adjust to an appropriate concentration for further use. Subsequently, bacteria samples ($OD_{600}=0.4$, 0.1 mL) were co-incubated with 3.9 mL tryptone soya broth (TSB) containing HA-NO-LF nanomicelles which had been stimulated by NO in a constant temperature shaker (37 °C, 120 rpm). In addition, the antimicrobial properties of PBS, LF and HA-NO-LF nanomicelles without exposure to NO were also assessed under the same procedure. The OD_{600} was monitored at intervals.

In addition, the four bacteria groups treated above were isolated and stained with propidium iodide (PI, 1 $\mu\text{g mL}^{-1}$) for 15 min, then stained with 4'-6-diamidino-2-phenylindole (DAPI, 5 $\mu\text{g/mL}$) for further 5 min in the dark. A fluorescence microscope (Olympus BX53, Japan) was employed to visualize the distribution of live and dead colonies.

2.7. Biocompatibility analysis

The cytotoxicity of nanomicelles was assessed against RAW 264.7 cells by MTT assay. The RAW 264.7 cells were first seeded in 96-well plates at a density of 1×10^4 cells/well in 200 μL of RPMI 1640 medium and incubated at 37 °C in a humidified atmosphere with 5% CO_2 for 24 h. The cells were then treated with HA-NO-LF nanomicelles (50, 100 and 200 $\mu\text{g/mL}$) respectively. PBS was used as blank control. After incubation for another 24 h, the culture medium was removed and 20 μL of MTT (5 mg/mL) was added into each well and incubated for 4 h at 37 °C. Subsequently, 100 μL DMSO was added to dissolve the dark blue formazan crystals generated by mitochondrial dehydrogenase in living cells. The optical density (OD) at 570 nm was monitored by a microplate reader (Perlong DNM-9062, Perlong New technology Co., Ltd, Beijing, China).

In order to determine the compatibility of HA-NO-LF nanomicelles with blood, the hemolysis assay was performed as described in our recent work (Lu et al., 2019). In brief, 0.2 mL of red blood cells (RBC) solution (2% w/w) was dispersed in 0.8 mL of HA-NO-LF nanomicelles (50, 100, 200 $\mu\text{g}/\text{mL}$). Pure water and PBS were used as positive controls (PC, 100% lysis) and negative controls (NC, 0% lysis), respectively. After incubation for 3 h at 37 $^{\circ}\text{C}$, the obtained mixtures were centrifuged at 6500 rpm for 10 min to remove unruptured cells. Then 200 μL supernatant was collected and measured by an automated microplate reader as mentioned above at 545 nm to record respective OD value.

$$\text{Hemolysis ratio (\%)} = (\text{OD}_{\text{sample}} - \text{OD}_{\text{NC}}) / (\text{OD}_{\text{PC}} - \text{OD}_{\text{NC}}) \times 100$$

The *in vivo* biosafety test was similar with a previous report (Wang et al., 2016).

2.8. Intracellular uptake of nanomicelles

To evaluate the intracellular uptake capacities of nanomicelles in RAW 246.7 cell lines, RAW 246.7 cells were first cultured in 6-well microplates in accordance with the previous report (J. Li et al., 2012). Then the culture media were replaced with media containing DIO-loaded HA-NO-LF nanomicelles (150 $\mu\text{g}/\text{mL}$). To investigate whether nanomicelles were specifically taken up by RAW 246.7 cells through HA-receptors mediated endocytosis, cells were preincubated with free-HA (4 mg/mL) for 2 h before adding the fluorescently-labeled nanomicelles. After co-incubation for 3 h, cells were washed with PBS buffer for three times and stained by DAPI (5 $\mu\text{g}/\text{mL}$) to label the cell nucleus. The cells were then imaged on a fluorescence microscopy (Olympus BX53).

2.9. Intracellular bacteria experiment

According to our previous work (Qiu et al., 2017), RAW 264.7 cells were co-incubated with *S. aureus* in a cell culture incubator for 1 h to establish an infection model *in vitro*. Then 50 $\mu\text{g}/\text{mL}$ of gentamicin was added to eradicate extracellular bacteria. Additionally, the cells were washed three times with PBS and then incubated in 1 mL fresh medium containing LF alone, HA plus LF, HA-NO-LF nanomicelles

and HA-NO-LF plus L-NAME (300 $\mu\text{mol/L}$) respectively. PBS was applied as blank control. After incubation for further 12 h at 37 $^{\circ}\text{C}$, the cells were lysed with Triton X-100. And colony forming unit (CFU) of intracellular bacteria in the lysates was recorded by counting live bacteria in tryptic soy agar (TSA) plates after serial dilution.

2.10. *In vivo* pharmacodynamic assessment

Firstly, female Kunming mice (weighing approximately 25 g) between 6 and 8 weeks of age were anesthetized with sodium phenobarbital at a dose of 30 mg/kg, then 10 μL of *S. aureus* (10^9 CFU/mL) was injected through weasand to establish the pneumonia model for further use.

To assess the therapeutic efficacy of HA-NO-LF nanomicelles *in vivo*, the mice were randomly assigned into four experimental groups: control, LF, HA plus LF and HA-NO-LF nanomicelles (n=7). Subsequently, the infected mice were treated with saline solution, LF, a simple mixture of HA and LF, HA-NO-LF nanomicelles (10 mg/kg) via tail vein injection respectively for three consecutive days. 24 h after the last treatment, the mice were sacrificed. Then the lungs of each group were separated and mashed into homogenate. The CFU of live bacteria in each organ was calculated with the same system as operated above. Furthermore, tissue sections were prepared according to conventional methods (Lou et al., 2018; C. Y. Zhang et al., 2019) to observe the level of inflammation.

To investigate the extent of nanomedicine accumulation in pathological site, DIO-loaded HA-NO-LF nanomicelles were injected to the infectious mice and lung homogenates were prepared at scheduled time intervals. The same DIO dose was administered for comparison. Then the fluorescence intensities of DIO were obtained by using a BRUKER TEMSOR 27 fluorescence spectrophotometer with an excitation wavelength of 480 nm.

2.11. Statistical analysis

Experimental data were expressed as mean \pm standard deviation (SD) and plotted

and statistically analyzed using the software GraphPad Prism 5.01.

3. Results and discussion

3.1. Synthesis and characterization of HA-NO-LF

The synthesis of HA-NO-LF was performed by following the synthetic route outlined in Fig.2. Formation of HA-NO-LF conjugate was confirmed by ^1H NMR and FTIR. As shown in Fig.3, the ^1H NMR of hybrids LF-NA-DP, the characteristic peaks of NH, aromatic hydrogens and vinyl hydrogen appear at $\delta = 12.94$ ppm, $\delta = 8.94$ - 7.43 ppm and 5.78 ppm, respectively. These signals are in full agreement with the target products. After the condensation reaction, the chemical shifts of NH and aromatic hydrogens of compound HA-NO₂-LF are in accordance with the signals of compound LF-NA-DP. Moreover, the signal of methyl group of the amide moiety appears at $\delta = 2.24$ ppm. After reduction, the chemical shifts of the antibiotic moiety and the methyl group of the amide moiety are observed at $\delta = 8.91$, 7.62 , 7.41 , 6.45 ppm and $\delta = 2.28$ ppm, which indicates the formation of HA-NO-LF. In the ^{13}C NMR spectra (Fig. S1), the characteristic peaks of the carbonyls appeared at 176.2 , 174.4 and 171.1 ppm. The chemical shifts of the aromatic carbons ranging from 155.7 ppm to 102.2 ppm, showed the presence of the aromatic rings. Further, the carbons of the hyaluronic acid and the aliphatic carbons showed multi-peaks ranging from 83.9 ppm to 18.6 ppm. The above information certified the formation of the conjugates. FTIR analysis was also used to verify the connection. As Shown in Fig. S2, the spectrum of LF-NA-DP revealed typical characteristic peaks for amide bond, such as a strong peak at 1571 cm^{-1} assigned to N-H bending vibrations, at 1293 cm^{-1} due to stretching of amines (C-N), indicating the successful conjugation of LF into NA-DP moieties. Similarly, The spectra of HA-NO₂-LF and HA-NO-LF showed sharp peaks of N-H moieties around 1571 cm^{-1} , which could also verify the connection as NMR claimed before.(Yang et al., 2010). UV spectra of HA, LF, and HA-NO-LF are shown in Fig.S3. There was no absorption peak of HA and an absorption peak of LF at 293 nm from 250 to 450 nm . HA-NO-LF showed an absorption peak at 295 nm . Compared to

LF, the absorption peak of HA-NO-LF was slightly red shifted (2 nm) due to the conjugation of amino in the NA-DP molecules with carboxide in the LF molecules. The esterification degree of free carboxyl acid in HA-NO-LF was 21.9%, according to the molar ratio of integration between N-acetyl and vinyl hydrogen. (Y. Zhang et al., 2019). UV-Vis measurement at 293 nm showed a drug content of 18.07 wt %, confirming successful synthesis of HA-NO-LF.

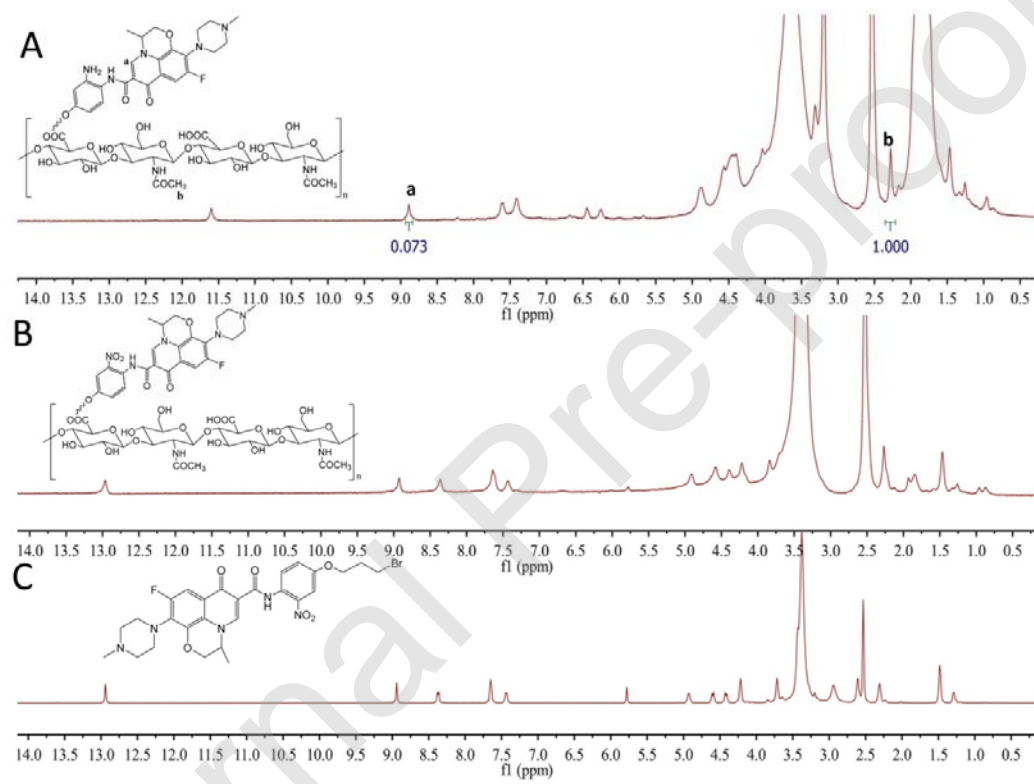


Fig. 3 ^1H NMR spectra of HA-NO-LF (A), HA-NO₂-LF (B), LF-NA-DP (C).

3.2. Characterization of HA-NO-LF nanomicelles

As shown in Fig. 4A, the size of HA-NO-LF nanomicelles was investigated by DLS to have an intensity-averaged hydrodynamic diameter of about 129 nm. It was supposed that the small particle size of nanomicelles could be ascribed to the effect of preformed hydrophobic unit acting as heterogeneous nucleation sites, which prevented the formation of larger particles during dialysis process. Besides, the nanomicells were found to partially carry negative charges according to Fig. 4B,

which might create favorable conditions for inducing electrostatic adsorption of the drug vehicle onto the surface of inflammatory sites, as demonstrated in previous studies (W. Li et al., 2018).

The micromorphology of HA-NO-LF nanomicelles was then performed using SEM, and the images are shown in Fig. 4C. In a view of Fig. 4C, the micelles were observed to exhibit well-separated individuals and a smooth surface. They were also found to remain sphere-like structures with diameter sizes around 120 nm, which was well corroborated with the results measured by DLS (Fig. 4A). The digital photo of nanomicelles was inserted in Fig. 4C (a), it was apparent that the nanomicelles showed a bright path once illuminated with a laser pointer, confirming the successful formation of the nanostructures once again.

To investigate storage stability of nanomicelles, the change of size distribution as well as zeta potential was monitored through 6 days using DLS measurement. As shown in Fig. 4D, with the function of time, the mean particle size of HA-NO-LF nanomicelles was essentially unchanged, similar to the result of zeta potential. The results described above confirmed the successful self-assembly and good stability of nanomicelles, avoiding abnormal release and inactivation of drug in normal storage conditions, which provided a promising prospect for the product to be applied as effective antibacterial agent.

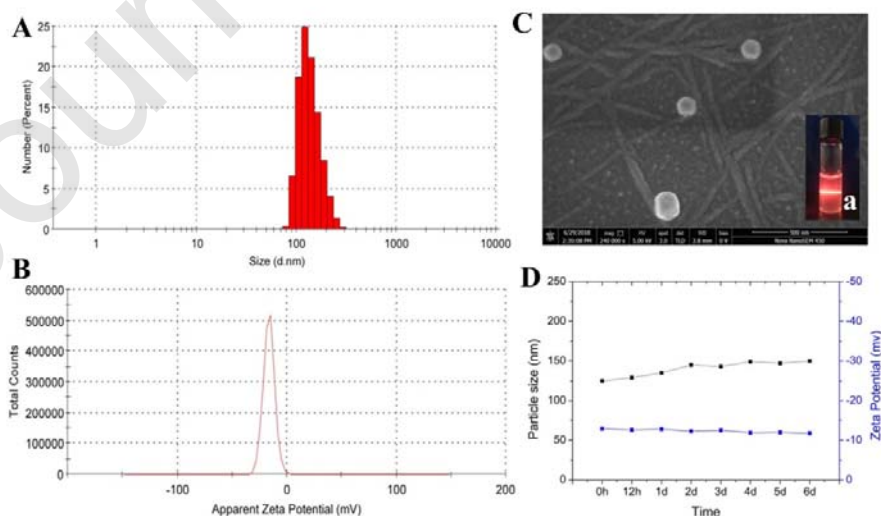


Fig.4 Particle size distribution curve (A), zeta potential (B) and SEM images (C) attached with an inset macroscopic image (a) of HA-NO-LF nanomicelles; Changes of particle size and zeta potential of HA-NO-LF nanomicelles after storing up to 6 days (D).

3.3. NO-triggered drug release *in vitro*

In order to confirm whether HA-NO-LF nanomicelles could achieve controlled release effect triggered by external NO, we performed NO-sensitive LF release experiments in a time-dependent manner in the presence and absence of NO. The release curve of LF showed in Fig. 5 exhibits a saltation once the NO was injected at 6 h (+ NO), indicating highly reactive nature of the nanomicelles. Upon extending the incubation time, the drug was released continuously in a highly efficient matter, as evident by a sharp release rate of LF between 6 to 15 h, achieving the total drug release efficiency at nearly 70%. By sharp contrast, there was no significant release of the drug in the group without NO stimulation with the function of time. It is noticeable, however, that the LF could also be detected for slight release without NO trigger (- NO), presumably attributed to the partial cleavage of nanomicelles affected by environment inevitably. Although only an initial proof of concept, the experiment above has demonstrated the potential of the HA-NO-LF nanomicelles to act as a drug delivery vehicle with sustained controlled release.

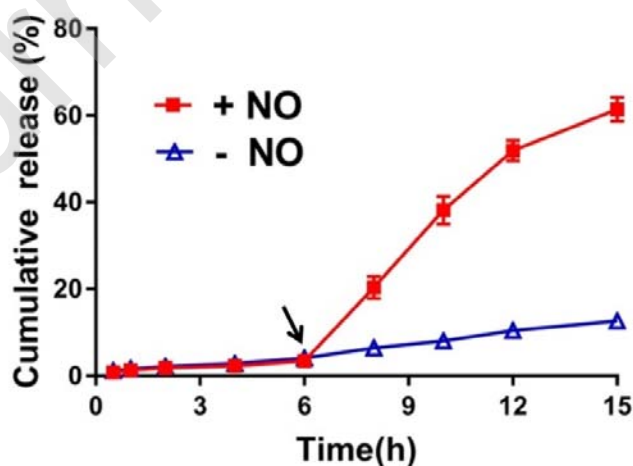


Fig.5 The time course of LF release profile of HA-NO-LF nanomicelles

in the presence and absence of NO.

3.4. *In vitro* antibacterial activity

A Gram-positive bacterium (*S. aureus*) was selected as the model bacteria to qualitatively analyze the antibacterial property of NO-sensitive nanomicelles, and the results were cheerfully presented in Fig. 6A, B. It is apparent that the HA-NO-LF nanomicelles exhibited almost no inhibition of bacterial growth compared with the blank control, which reveals the fact that LF was hardly cleaved from the nanomicelles in the absence of NO stimulus. Nevertheless, an unaltered OD value which tends to zero over time was observed (Fig. 6A) while treated by HA-NO-LF nanomicelles in the presence of NO, consistent with the antibacterial effect of pure LF. Besides, the macroscopic photos of colony growth shown in Fig. 6B revealed that the number of colonies decreased significantly when incubated with HA-NO-LF nanomicelles in the presence of NO, which provided powerful evidence supporting the successful cleavage and remarkable antibacterial effects of LF-loaded nanomicells. Meanwhile, the bactericidal effects of different mediations could also be clearly observed from the fluorescence microscopy images in Fig. S4 since the dead bacteria could be specifically dyed by PI. The discovery above showed conclusion that HA-NO-LF nanomicells could only possess the antibiotic effect when it came to contact with NO stimulus, which renders the NO-sensitive micelles suitable for intracellular delivery of drugs.

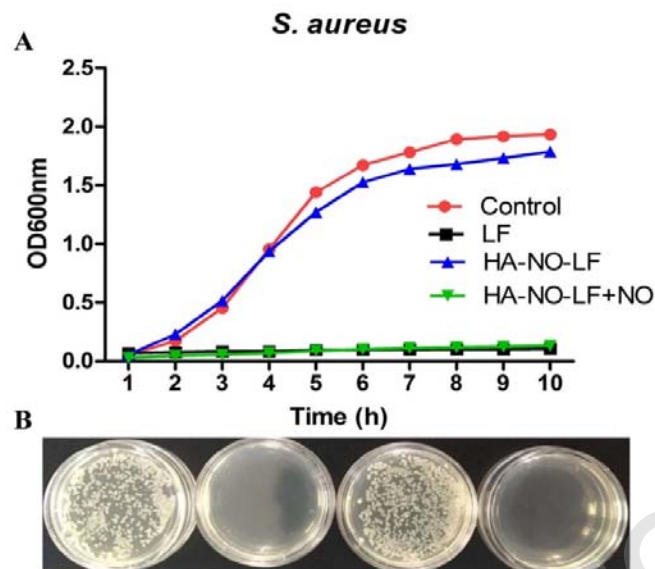


Fig.6 Growth curves of *S. aureus* cultured by PBS, LF, HA-NO-LF nanomicelles with and without exposure to NO, respectively (A); Macroscopic photos of colony growth above with different treatments (B).

3.5. Study on biocompatibility

It has been universally acknowledged that biosafety as well as biocompatibility are fundamental requirements for biomaterial. Then *in vitro* cytotoxicity of HA-NO-LF nanomicelles were investigated by MTT assays in RAW 246.7 cells. As depicted in Fig. 7A, the cell viability decreased slightly with the increase in the concentration of HA-NO-LF nanomicelles from 50 to 200 $\mu\text{g/mL}$. However, no significant toxicity (cell viability > 90%) was found in RAW 246.7 cells even at a high concentration of HA-NO-LF nanomicelles at 200 $\mu\text{g/mL}$. Moreover, assessing the interaction of intravenous preparations with blood components is also of great concern just in case pathophysiological events. The percentage of hemolysis was around 7% for the nanomicelles over a wide range of concentrations, revealing blood compatibility of HA-NO-LF nanomicelles (Fig. 7B) (Figueiredo et al., 2017). The potential acute toxicity of the nanomicelles was further assessed by analyzing tissue functions. As shown in Fig. S5, no significant difference between nanomicelles treated group and the control group treated with PBS, demonstrating negligible acute

toxicity of HA-NO-LF nanomicelles. In general, the multifunctional nanomicelles we designed are of good biocompatibility, which laid a solid foundation for subsequent *in vivo* experiments and practical applications in the future.

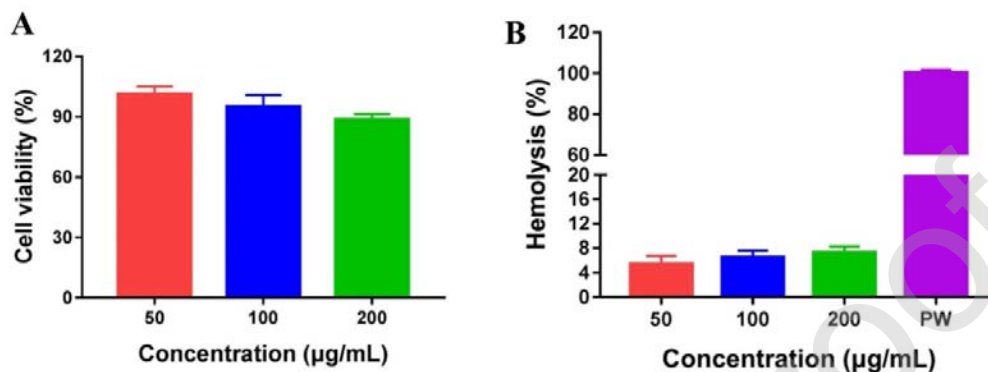


Fig.7 *In vitro* cytotoxicity of different concentrations of nanomicelles on RAW 246.7 cells (A); Hemolysis reaction of different concentrations of nanomicelles on red blood cells (B).

3.6. Intracellular uptake of nanomicelles

Having validated the desired chemical responsiveness of HA-NO-LF nanomicelles, we ulteriorly investigated cellular uptake of nanomicelles and competitive inhibition of specific receptors on the surface macrophages. DIO is a crucial stain which exhibits green fluorescence in cells, and DIO payload inside the nanomicelles was used as fluorescent marker to qualitatively analyze the amount of HA-NO-LF nanomicelles located in intracellular compartments.

As displayed obviously in Fig. 8A, strong green fluorescence was observed when RAW 246.7 cells incubated with the nanomicelles for 3 h, implying high intracellular uptake capabilities for the HA-NO-LF nanomicelles. When it comes to competition inhibition assay, the fluorescence intensity (green) of HA-NO-LF nanomicelles treated with free-HA was weaker to that of untreated one, while blue fluorescence which referred to cell nucleus of those two test groups remained almost the same intensity (Fig. 8A, B). It was suggested that free-HA could competitively interact with specific HA-receptors such as CD44 receptors, hindering the endocytosis mediated by HA-receptors of the HA-NO-LF nanomicelles and resulting in the decreased

fluorescent intensity (J. Li et al., 2012). This result appears to be consensus with our hypothesis that HA-NO-LF nanomicelles could be specifically adsorbed onto the surface of macrophages via receptor-mediated nature, facilitating nanomicelles passage through cytomembrane.

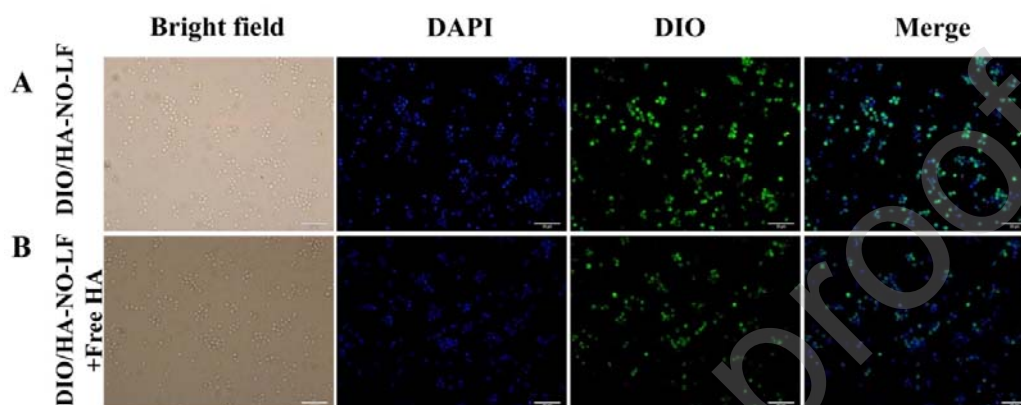


Fig.8 Confocal microscopy images of RAW 246.7 cell line incubated with DIO-loaded HA-NO-LF nanomicelles (A), and with free-HA polymer pretreated DIO-loaded HA-NO-LF nanomicelles(B). Scale bars correspond to 50 μm in all the images.

3.7. Intracellular bacteria experiment

On the basis of above results, we attempted to further explore the NO-sensitive performance under simulated biological inflammatory conditions. To investigate whether the nanomicelles are capable of responding to endogenous NO secreted from cells cultured *in vitro*, the RAW 264.7 cell was chosen as model cell since it is a type of murine macrophage that produces NO when infected by bacteria(Park et al., 2017).

As shown in Fig. 9, the intracellular bacteria were eliminated efficiently by LF, whereas the simple mixture of HA and LF didn't contribute to further decrease of CFU remained in infected cells. As such, it is conceivable that HA alone has no contribution to the antibacterial activity of testing groups. In addition, the HA-NO-LF nanomicelles group had a marked decrease in CFU value compared with single LF with the same effective dose of antibiotic. We could thus make a bold speculation that free LF can be transferred into cells by passive diffusion or dispersed in the liquid

medium without specific targeting, while HA-NO-LF nanomicelles could be internalized by endocytosis via HA receptors which were highly expressed by activated macrophages and then controlled release of effective LF, resulting in better therapeutic effect against intracellular bacteria.

To further confirm the NO-sensitive behavior of HA-NO-LF nanomicelles in activated macrophages, L-NAME was added to the macrophages to inhibit the production of NO (He & Frost, 2016). The result presented in Fig.8 is consistent with our conjecture that the bactericidal activity of HA-NO-LF nanomicelles was significantly decreased without stimulated by enough NO.

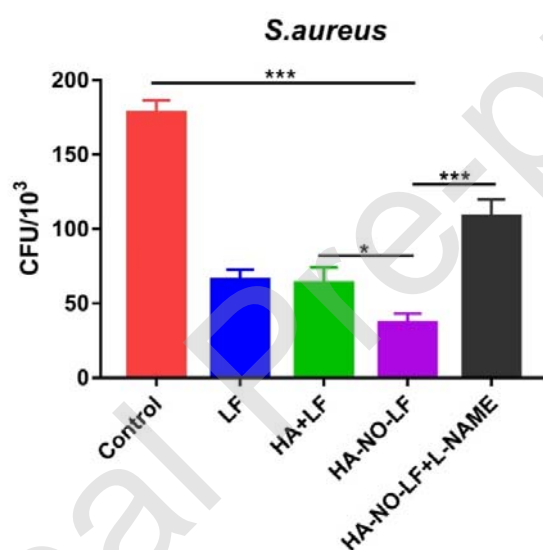


Fig. 9 RAW264.7 cells infected with *S. aureus* were treated with PBS, LF alone, simple mixture of HA and equivalent LF, HA-NO-LF nanomicelles, HA-NO-LF nanomicelles added with L-NAME, respectively. Values are given as the mean \pm SD of triplicates. * $p < 0.05$, ** $p < 0.005$, *** $p < 0.001$.

3.8. Therapeutic efficacy of HA-NO-LF nanomicelles *in vivo*

To evaluate *in vivo* antibacterial activities of the formulated drugs, the infected mice were tail-intravenously injected with various agents as vividly depicted in Fig. 10A. After drugs administration, various degrees of inhibition to the propagation of pathogenic bacteria compared with control group were observed in Fig. 10B. Notably,

the HA-NO-LF nanomicelles group showed more effective suppression of *S. aureus* than LF group, while the germicidal ability of tested group treated with simple mixture of HA and LF was equivalent to LF alone. Taken in this sense, the HA-NO-LF nanomicelles exhibited better antibacterial efficacy under the same content of LF compared with other groups. From histological analysis in Fig. 10C, the lung in mice treated with saline displayed obvious signs of inflammatory response, containing alveolar wall hyperemia and thickening. Specifically, the blood vessels were significantly dilated and part of the alveolar tissue structure collapsed to form abscesses in the alveolar cavity. Moreover, we found numerous inflammatory cells infiltrating the alveolar septum and spaces with hemorrhage and congestion. However, the group treated with HA-NO-LF nanomicelles decreased pathological tissue damage and showed lower pulmonary inflammatory characteristics compared with other groups. In addition, it is evident that the fluorescence intensity of DIO from the nanomicelles was significantly higher than that of free DIO at all three time points from 2 to 8 h (Fig. S6), which confirmed the accumulation of nanomicelles in pathological lung tissues. Taken together, these results indicated that HA-NO-LF nanomicelles could effectively reverse *S.aureus* infection *in vivo*.

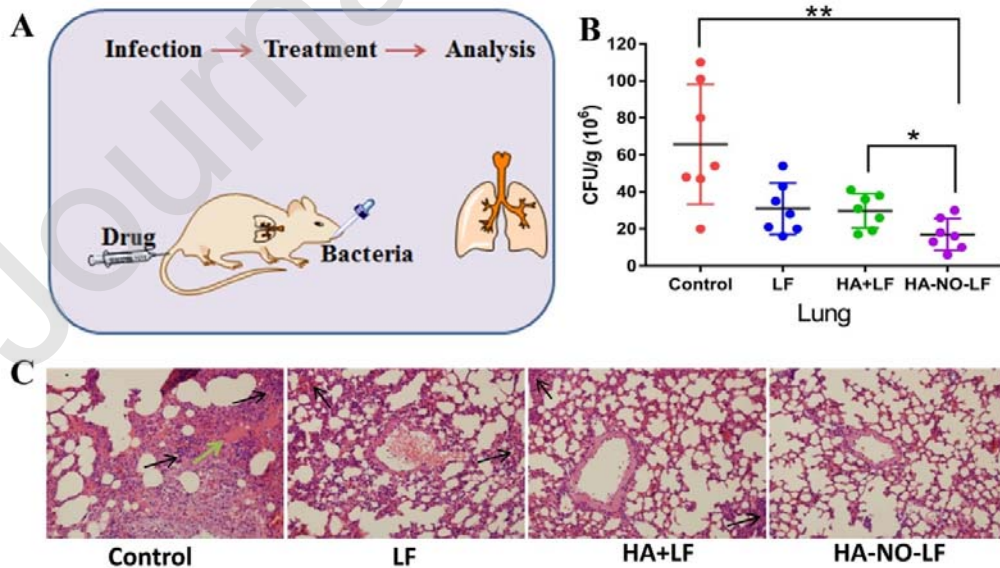


Fig.10 The schematic illustration about establishment and treatment of pneumonia model (A); Average CFU values recorded in lung tissues of four animal groups: control, LF, simple mixture of HA and LF and HA-NO-LF nanomicelles, respectively (B); Analysis in lung tissues of the impact of four experimental groups: control, LF, simple mixture of HA and LF, HA-NO-LF nanomicelles (C). The black arrows indicate that alveolar tissue collapse. The green arrows depict alveolar wall hyperemia. Values are given as the mean \pm SD of triplicates. * $p < 0.05$, ** $p < 0.005$, *** $p < 0.001$.

4. Conclusions

In this paper, the novel HA-based nanomicelles with NO-sensitive antibacterial properties was prepared by conjugating LF with HA using a functionalized intermediate bearing *o*-phenylenediamine groups. It was found *in vitro* that the nanomicelles were cleaved to release LF gradually and exerted great antibacterial effect against *S.aureus* upon exposure to NO. Meanwhile, the NO-triggered nanomicelles retained good biosafety as well as biocompatibility. The results of the competition inhabitation assay proved that the nanomicelles could enter macrophages via a CD44 mediated endocytosis. Moreover, *in vivo* pharmacodynamic assessment acknowledged their ability to fight against bacteria and reduce inflammatory levels. All these results suggested that NO-sensitive HA-based nanomicelles hold great promise as a targeting vehicle for selective delivery of drugs to pathogenic sites, thereby enhancing the therapeutic efficacy for infectious diseases.

5. Conflicts of interest

There are no conflicts of interest to declare.

6. Acknowledgements

This work was supported by the National Natural Science Foundation of China (NSFC) (31870799 and 31700707) and the Fundamental Research Funds for the Central Universities (2452017026). The authors are grateful to Life Science Research Core Services (LSRCS), Northwest A&F University for providing SEM measurement.

References:

- Chen, M., Xie, S., Wei, J., Song, X., Ding, Z., & Li, X. (2018). Antibacterial Micelles with Vancomycin-Mediated Targeting and pH/Lipase-Triggered Release of Antibiotics. *ACS Appl Mater Interfaces*, 10(43), 36814-36823.
- Coussens, L. M., & Werb, Z. (2002). Inflammation and cancer. *Nature*, 420(6917), 860-867.
- Figueiredo, P., Lintinen, K., Kiriazis, A., Hynninen, V., Liu, Z., Bauleth-Ramos, T., . . . Santos, H. A. (2017). In vitro evaluation of biodegradable lignin-based nanoparticles for drug delivery and enhanced antiproliferation effect in cancer cells. *Biomaterials*, 121, 97-108.
- Gao, W., Thamphiwatana, S., Angsantikul, P., & Zhang, L. (2014). Nanoparticle approaches against bacterial infections. *Wiley Interdisciplinary Reviews Nanomedicine & Nanobiotechnology*, 6(6), 532.
- He, W., & Frost, M. C. (2016). CellNO trap: Novel device for quantitative, real-time, direct measurement of nitric oxide from cultured RAW 267.4 macrophages. *Redox Biol*, 8, 383-397.
- Hoey, S., , Grabowski, P. S., Ralston, S. H., Forrester, J. V., & Liversidge, J., . (1997). Nitric oxide accelerates the onset and increases the severity of experimental autoimmune uveoretinitis through an IFN-gamma-dependent mechanism. *Journal of Immunology*, 159(10), 5132.
- Hu, J., Whittaker, M. R., Duong, H., Li, Y., Boyer, C., & Davis, T. P. (2014). Biomimetic polymers responsive to a biological signaling molecule: nitric oxide triggered reversible self-assembly of single macromolecular chains into nanoparticles. *Angew Chem Int Ed Engl*, 53(30), 7779-7784.
- Hu, J., Whittaker, M. R., Yu, S. H., Quinn, J. F., & Davis, T. P. (2015). Nitric Oxide (NO) Cleavable Biomimetic Thermoresponsive Double Hydrophilic Diblock Copolymer with Tunable LCST. *Macromolecules*, 48(12), 3817-3824.
- Huang, G., & Huang, H. (2018). Hyaluronic acid-based biopharmaceutical delivery and tumor-targeted drug delivery system. *J Control Release*, 278, 122-126.
- Li, J., Huo, M., Wang, J., Zhou, J., Mohammad, J. M., Zhang, Y., . . . Zhang, Q. (2012). Redox-sensitive micelles self-assembled from amphiphilic hyaluronic acid-deoxycholic acid conjugates for targeted intracellular delivery of paclitaxel. *Biomaterials*, 33(7), 2310-2320.
- Li, W., Li, Y., Liu, Z., Kersakundee, N., Zhang, M., Zhang, F., . . . Santos, H. A. (2018). Hierarchical structured and programmed vehicles deliver drugs locally to inflamed sites of intestine. *Biomaterials*, 185, 322-332.
- Liu, Q., Hu, J., Whittaker, M. R., Davis, T. P., & Boyd, B. J. (2017). Nitric oxide-sensing actuators for modulating structure in lipid-based liquid crystalline drug delivery systems. *J Colloid Interface Sci*, 508, 517-524.
- Lou, W., Venkataraman, S., Zhong, G., Ding, B., Tan, J. P. K., Xu, L., . . . Yang, Y. Y. (2018). Antimicrobial polymers as therapeutics for treatment of multidrug-resistant *Klebsiella pneumoniae* lung infection. *Acta Biomater*, 78, 78-88.
- Lu, C., Sun, F., Liu, Y., Xiao, Y., Qiu, Y., Mu, H., & Duan, J. (2019). Versatile Chlorin e6-based magnetic polydopamine nanoparticles for effectively capturing and killing MRSA. *Carbohydr Polym*, 218, 289-298.
- Ma, T., Zheng, J., Zhang, T., & Xing, D. (2018). Ratiometric photoacoustic nanoprobes for monitoring

- and imaging of hydrogen sulfide in vivo. *Nanoscale*, 10(28), 13462-13470.
- McDonald, B., & Kubes, P. (2015). Interactions between CD44 and Hyaluronan in Leukocyte Trafficking. *Front Immunol*, 6, 68.
- Mu, H., Liu, Q., Niu, H., Sun, Y., & Duan, J. (2016). Gold nanoparticles make chitosan–streptomycin conjugates effective towards Gram-negative bacterial biofilm. *RSC Advances*, 6(11), 8714-8721.
- Park, J., Pramanick, S., Kim, J., Lee, J., & Kim, W. J. (2017). Nitric oxide-activatable gold nanoparticles for specific targeting and photo-thermal ablation of macrophages. *Chem Commun (Camb)*, 53(81), 11229-11232.
- Qiu, Y., Hou, Y., Sun, F., Chen, P., Wang, D., Mu, H., . . . Duan, J. (2017). Hyaluronic acid conjugation facilitates clearance of intracellular bacterial infections by streptomycin with neglectable nephrotoxicity. *Glycobiology*, 27(9), 861-867.
- Sun, F., Zhang, P., Liu, Y., Lu, C., Qiu, Y., Mu, H., & Duan, J. (2019). A photo-controlled hyaluronan-based drug delivery nanosystem for cancer therapy. *Carbohydr Polym*, 206, 309-318.
- Tomišić, Z. B., Kujundžić, N., Krajačić, M. B., Višnjevac, A., & Kojić-Prodić, B. (2002). Molecular structures of new ciprofloxacin derivatives. *Journal of Molecular Structure*, 611(1), 73-81.
- Wang, Y., Ding, X., Chen, Y., Guo, M., Zhang, Y., Guo, X., & Gu, H. (2016). Antibiotic-loaded, silver core-embedded mesoporous silica nanovehicles as a synergistic antibacterial agent for the treatment of drug-resistant infections. *Biomaterials*, 101, 207-216.
- Xu, X., Saw, P. E., Tao, W., Li, Y., Ji, X., Bhasin, S., . . . Farokhzad, O. C. (2017). ROS-Responsive Polyprodrug Nanoparticles for Triggered Drug Delivery and Effective Cancer Therapy. *Adv Mater*, 29(33).
- Yang, S. J., Lin, F.-H., Tsai, K.-C., Wei, M.-F., Tsai, H.-M., Wong, J.-M., & Shieh, M.-J. (2010). Folic Acid-Conjugated Chitosan Nanoparticles Enhanced Protoporphyrin IX Accumulation in Colorectal Cancer Cells. *Bioconjug Chem*, 21(4), 679-689.
- Yeo, J., Lee, Y. M., Lee, J., Park, D., Kim, K., Kim, J., . . . Kim, W. J. (2019). Nitric Oxide-Scavenging Nanogel for Treating Rheumatoid Arthritis. *Nano Lett*.
- Zhang, C. Y., Lin, W., Gao, J., Shi, X., Davaritouchae, M., Nielsen, A. E., . . . Wang, Z. (2019). pH-Responsive Nanoparticles Targeted to Lungs for Improved Therapy of Acute Lung Inflammation/Injury. *ACS Appl Mater Interfaces*, 11(18), 16380-16390.
- Zhang, Y., Li, Y., Tian, H., Zhu, Q., Wang, F., Fan, Z., . . . Hou, Z. (2019). Redox-Responsive and Dual-Targeting Hyaluronic Acid-Methotrexate Prodrug Self-Assembling Nanoparticles for Enhancing Intracellular Drug Self-Delivery. *Mol Pharm*, 16(7), 3133-3144.